Radiochim. Acta **95**, 25–32 (2007) / **DOI** 10.1524/ract.2007.95.1.25

Trace element immobilization by uranyl minerals in granite-hosted uranium ores: Evidences from the Xiazhuang ore field of Guangdong province, China

By L. Lu[1], F. Chen[1,*], R. C. Ewing[2] and R. Wang[3]

[1] Guangzhou Institute of Geochemistry, Chinese Academy of Sciences, Guangzhou 510640, P.R. China
[2] Geological Sciences, The University of Michigan, Ann Arbor, MI 48109-1005, USA
[3] State Key Laboratory for Mineral Deposits Research, Nanjing University, Nanjing 210093, P.R. China

(Received January 18, 2006; accepted in revised form July 25, 2006)

Uraninite alteration / Trace element immobilization / Uranyl mineral paragenesis / Source-term estimation / Spent UO_2 *fuel / Geological disposal*

Summary. The oxidative alteration of uraninite and the fate of trace elements (Y, LREE, Zr, and Th) in a granite-hosted uranium ore deposit in north Guangdong province, China, were investigated to understand the geochemical behavior of spent UO_2 fuel and associated fission products and transuranium elements under oxidizing conditions. In light of the paragenetic relationship of the alteration products, two alteration series of uraninite were identified: one is the silicate series with a mineral paragenesis of uraninite → uranyl oxide hydrates → Si-rich uranyl phase → uranophane ($Ca[(UO_2)(SiO_3OH)]_2(H_2O)_5$), and the other is the phosphate series with a mineral paragenesis of uraninite → uranyl oxide hydrates → autunite ($Ca[(UO_2)(PO_4)]_2(H_2O)_6$) → yingjiangite ($(K_2, Ca)(UO_2)_7(PO_4)_4(OH)_6(H_2O)_6$). In contrast to the wide distribution and abundance of uranophane and the uranyl phosphate minerals, uranyl oxides were only occasionally found in the ore samples, suggesting that the uranyl silicates and phosphates should be the predominant alteration products of UO_2 under oxidizing conditions, although uranyl oxide hydrates would be the solubility-limiting phase of uranium in the very early stage of alteration. Furthermore, the interlayer cation of the uranyl phases in the Xiazhuang uranium ore field is dominated by Ca^{2+}, indicating that the release of uranium and other radionuclides will be limited mainly by uranophane and autunite during the oxidative alteration of spent UO_2 fuel in underground repositories where enhanced calcium concentration is expected due to cement/water reactions.

Compositionally, the cation atomic ratios in uranyl phases often deviate considerably from their respective stoichiometric values as indicated by the nominal formulae, but the compositional variation does not result in significant structural change as indicated by X-ray diffraction patterns. This observation indicates that the structure of U^{6+} minerals may easily be adjusted to accommodate impurity elements including crystallographically compatible radionuclides. Compared with the primary uraninites, the secondary minerals are slightly enriched in light REE, but significantly depleted in Y^{3+} probably due to its cation-radius mismatch with interlayer Ca^{2+}. The apparent enrichment of Zr^{4+} in uranophane and uranyl phosphates relative to uraninite may result from the coupled substitutions: $Zr^{4+} \leftrightarrow U^{6+}$ and $REE^{3+} \leftrightarrow Ca^{2+}(K^+)$. Because an adequate charge-balance mechanism and significant distortion of the coordination polyhedra are required for the substitution $An^{4+} \leftrightarrow U^{6+}$, this type of substitution may not be common.

1. Introduction

Nuclear fuel consists predominantly of UO_2 with approximately 4% fission products and actinides after a burn up of 40 MWd/kg U [1, 2]. UO_2 is unstable in an oxidizing environment, especially that involving radiolytically produced oxidants, and will rapidly alter to form a wide variety of U^{6+} phases [3–6]. Thus, large amounts of long-lived radionuclides would be released in a very short period due to the rapid alteration of spent UO_2 fuel. Therefore, predicting the geochemical behavior of radionuclides during the oxidative alteration of spent UO_2 fuel has long been a major interest for the performance assessment of nuclear waste repositories [7–11].

The possible incorporation of long-lived radionuclides into secondary uranyl phases has been discussed by a few authors [12–14]. The resultant near-field immobilization would enhance confidence in the concept of geological isolation for spent nuclear fuel, and is important to the source-term estimation for performance assessment of spent fuel as a waste form. Both the solution concentration of uranium and the secondary phase immobilization of actinides and fission products depend largely on the structure and stability of the secondary phases formed. Hence, it is important to predict the paragenesis of uranyl phases that would form in the near-field geochemical environment. One of the most challenging aspects of nuclear waste isolation is the extrapolation of short-term laboratory data to the long periods (thousands to millions of years). Fortunately, the alteration and paragenesis of natural minerals can be used as an analogue to predict the long-term behavior of waste forms and associated radionuclides [15]. The use of uraninite, UO_{2+x}, together with its impurities as a chemical and structural analogue for the analysis of the long-term behavior of UO_2 fuel

*Author for correspondence (E-mail: frchen@gig.ac.cn).

has been examined by many authors [16, 17], and its alteration products have been studied in a variety of geochemical environments [18–23]. The uranium ore in the Xiazhuang region of Guangdong province, China, is hosted by granitic rocks [24]. We examined and characterized the alteration of uraninite and the immobilization of trace elements by the secondary uranyl minerals in the Xiazhuang uranium ore deposit, the aim of which was to (1) promote our confidence in predicting the behavior of UO_2 fuel in granite-hosted repositories, and (2) improve our knowledge of the possible capacity and mechanisms of incorporation of radionuclides into the uranyl phases.

2. Geology

The Xiazhuang uranium ore deposit is located in the eastern part of the Guidong intrusive complex. This deposit is one of the largest granite-hosted uranium ore fields in China and is composed of several deposits (*e.g.*, 330, 331, 332, 333, 337). Frequent magmatic activities in the late Mesozoic era resulted in the emplacement of the Guidong intrusive complex which extends $E-W$ and is composed of a granitic batholith, two granitic stocks and numerous basic-intermediate dikes. The age of the batholith and the granitic stocks is 180–194 Ma and 145–155 Ma, respectively, while that of the basic-intermediate dikes is 90–110 Ma [25].

The Xiazhuang uranium ore deposit is of hydrothermal origin related to the late-phase Mesozoic magmatism, with the uranium mineralization being favored by the intersection of NNE- and EW-trending faults. The mineralization was tentatively divided into an early high-temperature stage (122–138 Ma) and a late intermediate-low temperature stage (54–96 Ma) [26, 27], and the major uranium mineralization occurred in the late stage [25]. The high-temperature minerals include uraninite, scheelite, fluorite, epidote, chlorite, tourmaline, rutile, zircon, apatite, biotite and pyrite [28], while the intermediate-low temperature hydrothermal activity is responsible for the formation of the mineral assemblage of uraninite, pyrite, chalcopyrite, galena, sphalerite, hematite and quartz [25].

Intensive alteration has developed on the uraninite in the Xiazhuang ore field due to groundwater infiltration. In addition to the uranyl oxide hydrates and uranyl silicates that are commonly found as oxidative alteration products, abundant uranyl phosphates have been found. Thus, the Xiazhuang uranium ore field is an ideal site for studying the behavior of UO_2 in a natural, oxidizing environment.

3. Sampling and analytical methods

Eighteen uranium ore samples that experienced different degree of oxidative alteration were obtained from 4 deposits. Polished sections of these samples were examined using optical microscopy, back-scattered electronic (BSE) images and electronic microprobe analysis (EMPA) to identify uranium minerals, analyze their paragenetic relationship and chemical composition. EMPA data and BSE images were obtained using a JEOL JXA 8800 M Superprobe operated at an accelerating voltage of 20 kV and a sample current of 20 nA. Appropriate silicate, oxide, and phosphate standards were used for calibration of the intstrument. The chemical formulae of uranium minerals were calculated based on the EMPA data using the procedure developed by Zhao and Ewing [21], except that Pb^{2+} in the secondary U^{6+} minerals was not considered to be radiogenic because these minerals are believed to be formed within no more than a few thousand years. In addition, some uranium minerals were characterized by X-ray diffraction analysis (XRD).

4. Results and discussion

4.1 Characterization of uranium minerals

The uranium minerals examined and analyzed in this study include uraninite, schoepite, becquerelite, calciouranoite, fourmarierite, uranophane, autunite and yingjangite. The uranyl minerals can be grouped into different types (uranyl oxide hydrates, uranyl silicates and phosphates). Average electron microprobe analysis of bulk composition for the primary and secondary uranium minerals, together with the calculated formulae, is listed in Table 1, and the average trace element content is listed in Table 2.

4.1.1 Uraninite

The uraninite in Xiazhuang uranium ore field occur as a primary uranium mineral in veinlets of less than 2 mm wide or as disseminated grains, and was observed in 5 samples. Uraninite is usually associated with primary calcite, fluorite, apatite, pyrite, galena and sphalerite, and is often replaced by secondary uranyl minerals along grain boundaries and fractures. The uraninite often has embayed grain boundaries, pits and web-like fractures, and sometimes occurs as alteration relicts (Figs. 1a, 2a), indicative of intensive oxidative alteration and dissolution. Many disseminated uraninite grains are surrounded by brownish halos which were proposed to result from gamma radiolysis [29].

Uraninite has a nominal composition close to UO_{2+x} and contains varying amounts of ThO_2, ZrO_2, REE_2O_3 and some other metal oxides as impurities [17, 30]. The oxidation state of uranium which is indicated by U(IV)/U(VI) ratio, varies significantly for the uraninite in the Xiazhuang ore field with its composition ranging from $UO_{2.1}$ to U_3O_8 as calculated using EMPA results. Similar phenomena have also been observed in many other deposits, such as Oklo of Gabon, the Athabasca Basin of Saskatchewan and the Colorado Plateau [21, 29, 31]. Crystallographic evidence suggests that uraninites are most probably a mixture of two phases, $UO_{2.00-2.07}$ and $UO_{2.23-2.25}$ [32], while naturally occurring uraninite formed at low-temperatures usually has compositions ranging from $U_{2.5}$ to U_3O_8 [33]. Thus, the large variation in the oxidation state of uranium may result from the large variation of temperature at which uraninites formed. Lead content varies from 0.06 to 2.89 wt. %, and is assumed to be radiogenic due to uranium decay. The uraninites have incorporated Y and lanthanides as impurities with Y_2O_3 content averaging 0.35 wt. % (0.28 ∼ 0.47%), while the content of ThO_2 and ZrO_2 is very low and usually below detection limits (∼ 0.01 wt. %).

Table 1. Bulk chemical composition of uranium minerals.

Mineral	No. of analyses	Content	UO_2 (%)	CaO (%)	PbO (%)	SiO_2 (%)	P_2O_5 (%)	Na_2O (%)	K_2O (%)	Al_2O_3 (%)	$\sum 1$ (%)	$\sum 2$ (%)	$\sum 3$ (%)
Uraninite	38	range	88.82–95.42	0.73–5.37	0.06–2.89	0.00–0.28	0.01–0.42	0.03–0.32	–	0.00–0.15	94.88–98.65	95.18–99.05	100
		average	91.10	2.52	1.39	0.11	0.36	0.19	–	0.07	95.74	96.02	100
Schoepite	4	range	85.42–90.29	0.00–2.86	0.65–3.72	0.00–0.46	0.00–0.12	0.00–0.40	–	–	89.58–94.06		94.11–99.37
		average	88.75	0.96	1.86	0.18	0.06	0.18	–	–	92.38		97.64
Becqerelite	3	range	85.71–87.50	3.32–3.93	1.47–1.79	0.00–1.21	0.03–0.05	0.16–0.25	–	–	93.53–94.54		98.03–99.03
		average	86.65	3.60	1.66	0.42	0.04	0.21	–	–	93.89		99.03
Calcioranite	4	range	80.59–83.26	6.04–9.49	2.18–4.11	0.00–0.40	0.00–0.03	0.04–0.28	–	–	92.24–93.43		96.21–99.04
		average	81.89	7.14	2.94	0.10	0.01	0.19	–	–	92.73		97.58
Fourmarier-ite	4	range	74.49–79.63	0.95–2.13	9.12–16.45	0.05–0.17	0.08–0.19	0.01–0.05	–	0.00–0.01	92.69–95.26		94.23–99.23
		average	78.91	1.74	12.77	0.08	0.14	0.02	–	0.00	94.24		98.91
Si-rich uranyl phase	4	range	80.01–81.80	5.63–6.02	0.33–1.59	0.80–5.85	0.11–0.15	0.06–0.26	–	–	94.01–95.43		98.10–99.33
		average	81.41	5.83	1.15	5.28	0.14	0.04	–	–	94.75		98.57
Uranophane	40	range	66.11–73.15	4.51–7.05	0.02–0.87	12.26–20.35	0.01–0.94	0.00–0.05		0.00–1.53	91.44–95.96		95.36–99.95
		average	68.12	6.04	0.31	17.72	0.48	0.03	0.07	0.41	93.18		97.22
Autunite	42	range	66.25–68.40	5.24–6.85	0.00–0.03	0.00–1.50	16.45–19.67	0.01–0.25	0.00–0.52	0.00–0.03	89.57–95.67		93.56–99.72
		average	67.25	6.17	0.11	0.36	17.70	0.07	0.14	0.02	91.82		95.81
Yingjiangite	29	range	72.43–75.14	1.46–2.29	0.01–0.20	0.00–1.88	10.35–10.93	0.01–0.22	0.07–1.20	0.00–0.20	86.13–91.40		90.44–96.69
		average	73.24	2.14	0.11	0.50	10.67	0.08	0.64	0.06	87.44		91.87

$\sum 1$ all oxides from EMPA;
$\sum 2$ after Pb in uraninite converted to UO_2;
$\sum 3$ after UO_2 recalculated to UO_2 and UO_3;
– undetected item.

Table 2. Content of selected trace elements for uranium minerals.

Phase	No. of analyses	Content	Y_2O_3 (%)	ZrO_2 (%)	La_2O_3 (%)	Ce_2O_3 (%)	Pr_2O_3 (%)	Nd_2O_3 (%)	Sm_2O_3 (%)	Eu_2O_3 (%)	Gd_2O_3 (%)	$\sum$LREE (%)
Uraninite	38	range	0.28–0.47	0.00–0.01	0.00–0.00	0.02–0.17	0.01–0.07	0.05–0.10	0.00–0.09	0.00–0.14	0.06–0.23	0.32–0.56
		average	0.31	0.00	0.00	0.10	0.01	0.07	0.02	0.08	0.13	0.41
Uranyl Hydroxide	15	range	0.11–0.46	0.00–0.03	0.00–0.00	0.05–0.13	0.00–0.13	0.03–0.16	0.00–0.08	0.04–0.16	0.02–0.43	0.29–0.93
		average	0.18(0.20)	0.01(0.01)	0.00(0.00)	0.10(0.11)	0.05(0.05)	0.05(0.05)	0.03(0.03)	0.08(0.09)	0.14(0.15)	0.45(0.50)
Uranophane	40	range	0.01–0.07	0.00–0.03	0.00–0.00	0.02–0.26	0.00–0.10	0.00–0.13	0.00–0.11	0.00–0.19	0.03–0.27	0.20–1.00
		average	0.03(0.04)	0.01(0.02)	0.00(0.00)	0.08(0.10)	0.04(0.05)	0.06(0.08)	0.03 (0.04)	0.07(0.10)	0.09(0.13)	0.37(0.50)
Autunite	43	range	0.00–0.06	0.02–0.05	0.00–0.00	0.01–0.08	0.00–0.09	0.01–0.11	0.00–0.10	0.02–0.18	0.02–0.26	0.07–0.65
		average	0.02(0.03)	0.03(0.04)	0.00(0.00)	0.04(0.06)	0.06(0.08)	0.04(0.06)	0.04(0.05)	0.08(0.11)	0.10(0.13)	0.36(0.49)
Yingjiangite	29	range	0.02–0.10	0.01–0.03	0.00–0.15	0.04–0.22	0.00–0.05	0.04–0.44	0.00–0.04	0.03–0.08	0.02–0.10	0.20–0.96
		average	0.04(0.06)	0.02(0.03)	0.03(0.04)	0.10(0.12)	0.03(0.04)	0.09(0.12)	0.02(0.02)	0.04(0.06)	0.06(0.07)	0.37(0.47)

The numbers in the parentheses are uranium normalized average contents.

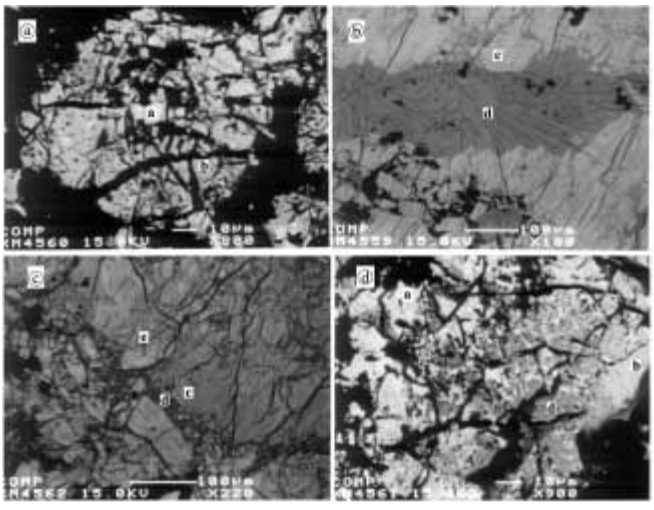

Fig. 1. Backscattered electron images of uraninite and its alteration products of silicate series in Xiazhuang ore deposit. (**a**) fractured uraninite partially replaced by uranyl hydroxide (calciouranoite). (**b**) Si-rich uranyl phase partially replaced by uranophane. (**c**) uranophane replacing Si-rich uranyl phase along fractures, with residual becquerelite in the Si-rich uranyl phase. (**d**) uraninite that is partially replaced by calciouranoite and uranophane. a-uraninite, b-Calciouranoite, c-Si-rich uranyl phase, d-uranophane, e-becquerelite.

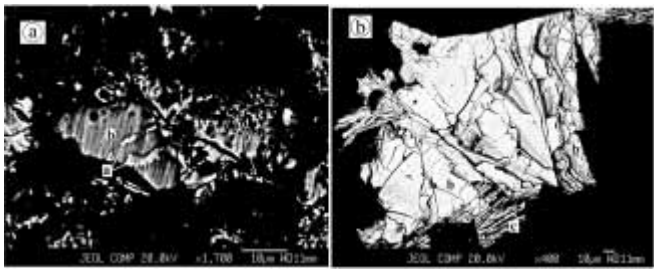

Fig. 2. Backscattered electron images of uraninite and its alteration products of phosphate series in Xiazhuang ore deposit. (**a**) uraninite residual in autunite. (**b**) yingjiangite at the margin of autunite. a-uraninite, b-autunite, c-yingjingite.

4.1.2 Uranyl oxide hydrates

Uranyl oxide hydrates are occasionally found in the studied ore samples as alteration products of uraninite, and have been found to consist of schoepite, becquerelite, calciouranoite and fourmarierite. These minerals generally replace primary uraninite along grain boundaries and fractures (Fig. 1a), and are replaced by uranophane (Figs. 1c and d).

Metaschoepite

The nominal composition of schoepite is $[(UO_2)_8O_2(OH)_{12}](H_2O)_{12}$. schoepite is a common alteration product of uraninite, but was identified only in sample 330-8 of this study. The schoepite is fine grained with a maximum grain size of $2 \sim 4\,\mu m$. Its average EMPA total is 97.64%, and the UO_3 content is 94.01%, belonging to strongly dehydrated polytypes of schoepite. The average content of PbO and CaO is 1.86% and 0.96%, respectively, and that of SiO_2, P_2O_5 and Na_2O are less than 0.2%. The Gd_2O_3 content is significant (up to 0.14%), while other trace elements are low or below detection limits.

Becquerelite

Becquerelite, $Ca[(UO_2)_3O_2(OH)_3]_2(H_2O)_8$, is the most abundant naturally occurring calcium uranyl oxide hydrate. A Ca-bearing uranyl phase was found in sample 330-1. It has a Ca : U atomic ratio of 1 : 5.1, which is close to that of becquerelite. This phase contains an average of 1.66 wt. % PbO, up to 0.46 wt. % Y_2O_3, up to 0.43 wt. % Gd_2O_3 and minor (< 0.2 wt. %) SiO_2, P_2O_5 and Na_2O.

Calciouranite

A Ca-rich uranyl oxide hydrate with a (Pb + Ca) : U atomic ratio of 1 : 2.2 was identified in sample 337-2. Its (Pb + Ca) : U atomic ratio is close to that indicated by the nominal composition of calciouranoite, $(Ca, Ba, Pb)U_2O_7(H_2O)_5$, and it is chemically similar to the calciouranoite identified by Zhao and Ewing (2000), with high PbO (2.96 wt. %) content.

Fourmarierite

Fourmarierite, $Pb[(UO_2)_4O_3(OH)_4](H_2O)_4$, is a common uranyl phase due to the high Pb content in uranium ores. A Pb-rich uranyl oxide hydrate was found only in one sample of this study, the average Pb : U atomic ratio of which is 1 : 5. Considering the high content of CaO (1.74 wt. %) which likely replaces PbO in the crystal structure, this phase is chemically closest to fourmarierite of all the Pb-rich uranyl oxide hydrates. The fourmarierite contains Y_2O_3 0.11%, Ce_2O_3 0.12%, Eu2O3 0.16%.

4.1.3 Uranyl silicates

Uranophane

Uranophane is one of the most abundant uranyl minerals in the studied ore deposit and was identified in 5 samples exhibiting different degree of alteration. It occurs as crystalline yellow powder in hand specimens, while BSE images show that radial aggregates are common. The distribution of uranophane around uranyl oxide hydrates or along the polygonal fractures in uranyl oxide hydrates and a Si-rich uranyl phase (see below) has been observed (Figs. 1b and c). Dehydration contraction of uranophane is evidenced by the appearance of web-like fractures in coarse grains, and confirmed by the high EMPA total of $91.44 \sim 95.96$ wt. %. The bulk composition is $12.26 \sim 20.35$ wt. % SiO_2, $66.11 \sim 73.15$ wt. % UO_2, and $4.51 \sim 7.05$ wt. % CaO, with Ca : Si : U atomic ratios in the range of $(0.29 \sim 0.52) : (0.74 \sim 1.36) : 1.0$, closest to those of uranophane, $Ca[(UO_2)(SiO_3OH)]_2(H_2O)_5$, of all uranyl silicates. A uranyl silicate phase in sample 333-0 has an average Si : U ratio of 1.33 : 1, but exhibited identical XRD pattern to uranophane. As compared with uraninites and uranyl oxide hydrates, the uranophane has higher Ce_2O_3 (up to 0.26%) and Gd_2O_3(up to 0.11%) contents and significantly lower PbO and Y_2O_3 contents.

4.1.4 Si-rich uranyl phase

This phase was found in sample 330-1 (Figs. 1b and c) and is associated with uranophane. Meanwhile, relicts of uranyl oxide hydrates were observed, and two types of fracture were developed in this phase. Of the two fracture groups, one is filled by uranophane and the other extends into the uranophane. These observations indicate that it formed prior to uranophane by replacing uranyl oxide hydrates. This phase contains $4.80 \sim 5.75$ wt. % SiO_2, $80.01 \sim 83.53$ wt. % UO_2 and $5.63 \sim 6.02$ wt. % CaO, with significant amount of PbO ($0.83 \sim 1.59\%$), Y_2O_3 ($0.50 \sim 0.55\%$) and P_2O_5 ($0.11 \sim 0.15\%$). It is compositionally intermediate to becquerelite and uranophane, and could be crystallographically transitional.

4.1.5 Uranyl phosphates

The Xiazhuang uranium ore field is characterized by the wide distribution of uranyl phosphates that are dominated by autunite and yingjangite. These two uranyl phosphates were identified in 10 of the 18 samples and show higher abundance close to the fractures intersecting the uranium ore. Other uranyl phosphates were not found in this study. They usually associate with uraninite and uranyl oxide hydrates, but have never been observed to associate with uranyl silicate minerals. Relicts of uraninite or uranyl oxide hydrates were found within autunite, and yingjangite occurs in intergranular spaces of autunite (Fig. 2b). These observations suggest that autunite formed prior to yingjangite at the expense of uranyl oxide hydrates and uraninites.

Autunite

A green sheet mineral was found filling faulted fractures and cavities, the XRD pattern of which is identical to that of autunite. A morphologically and compositionally similar phase was also identified in the ore matrix of at least 5 samples by BSE images and EMPA. The chemical composition of the autunite is UO_2 $66.25 \sim 68.4\%$, P_2O_5 $16.9 \sim 19.67\%$ and CaO $5.86 \sim 6.85\%$, with the Ca : P : U atomic ratios $(0.42 \sim 0.49) : (0.97 \sim 1.09) : 1$, very close to the stoichiometric ratios of autunite, $Ca[(UO_2)(PO_4)]_2(H_2O)_6$. In addition, minor SiO_2 (up to 1.50 wt. %), Nd_2O_3 and Gd_2O_3 are incorporated into the structure of the autunite, and PbO is generally below the detection limit.

Yingjangite

Yingjangite, $(K_2, Ca)(UO_2)_7(PO_4)_4(OH)_6(H_2O)_6$, was first discovered by Chen *et al.* (1990) [34] in the Yingjiang region of Yunnan province, China, and was reported to occur in the Xiazhuang uranium ore field by Zhang *et al.* (1992) [35]. The bright yellow and saffron yellow acicular crystals in

samples 330-4 and 330-7 are yingjangite as identified by XRD analysis in this study. Meanwhile, EMPA data indicate that it occurs also in a few of other samples. The major components of yingjiangite include UO_2, P_2O_5, CaO, and K_2O (Table 1), with their contents similar to the data for yingjiangite reported by Chen *et al.* (1990) and Zhang *et al.* (1992), except that the K_2O content is lower. The yingjiangite contains high SiO_2 (up to 1.88%), low PbO ($0.05 \sim 0.11\%$), high Ce_2O_3 (up to 0.22%) and Nd_2O_3 (up to 0.44%).

4.2 Paragenesis of uranyl minerals

The occurrences of the uranyl minerals in the Xiazhuang ore field demonstrate that they are alteration products of uraninite in an oxidizing environment caused mainly by the infiltration of aerated groundwater. During the alteration, the oxidized uranium was initially hydrolyzed to form schoepite and calcium uranyl oxide hydrates. The uranyl oxide hydrates were penetrated and partially replaced by uranophane, or occur as relicts in the Si-rich uranyl phase and autunite. The association of uranyl silicates with uranyl phosphates was not observed, which suggests that the oxidative alteration of uraninite could be divided into a silicate series and a phosphate series in the Xiazhuang ore deposit depending on the local geochemical environment of alteration. The penetration of uranophane in the Si-rich uranyl phase indicates that uranophane is the most stable phase in the silicate alteration series, and the observation that yingjangite occurs in intergranular spaces of autunite suggests that yingjangite should be the most stable phase in the phosphate series. Therefore, the paragenetic sequence of the silicate and phosphate alteration series could be summarized, respectively, as: uraninite → uranyl oxide hydrates → Si-rich uranyl phase → uranophane, and uraninite → uranyl oxide hydrates → autunite → yingjiangite. This observation agrees with the general recognition that an initial decomposition of UO_{2+x} to uranyl oxide hydrates was followed by the formation of more stable uranyl silicates or, in phosphorus-rich groundwaters, the formation of uranyl phosphates [3, 4]. Thermodynamic considerations also demonstrate that the groundwaters from crystalline rocks plot in uranyl silicate stability fields in the SiO_2-CaO-UO_3-H_2O system [36]. A further examination of the data reveals that (1) uranyl silicate and uranyl phosphate dominate the alteration products of uraninite in the Xiazhuang ore deposit with minor uranyl oxide hydrates each occurring only in one or two samples; and (2) Ca^{2+} is the predominant interlayer cation in the uranyl minerals.

In summary, uranyl oxide hydrates are unstable but may be kinetically favored early during the corrosion of uraninite. The existence of metastable phases has largely complicated the uranyl mineral assemblages in natural systems and lessened our confidence in predicting the predominant phase(s) that would form as alteration products of spent UO_2 fuel in underground repositories. Another major source of uncertainty in the prediction based on natural analogue studies may be the compositional difference between uraninite and spent UO_2 fuel. As an example, in contrast with the spent UO_2 fuel, natural uraninites, especially those hundreds of millions years old, usually contains significant amount of radiogenic lead, which may result in the formation of a large amount of lead-bearing uranyl phases and prohibits the formation of the uranyl phases that would have formed in the absence of radiogenic lead.

According to thermodynamic considerations, the kinetically favored metastable phases can only partially be preserved at locations that are not accessible by groundwater. This argument is confirmed by the predominance of thermodynamically stable uranyl phases in the alteration products of uraninite observed in this study and many other studies. Uranyl silicates have been observed to form within two years in the alteration experiments of UO_2 at 90 °C which is close to the temperature expected in nuclear waste repositories when the waste package fails [37]. Moreover, autunite has been observed to directly replace uraninite with the absence of metastable mineral phases. Thus, the metastable uranyl phases may control the solubility of uranium only in the very early of less than a few years after the exposure of spent UO_2 fuel to groundwater. In addition, Pb-bearing uranyl phase can be precluded in the alteration products of UO_2 fuel due to low lead content in the near-field. Considering the predominance of Ca-bearing uranyl minerals in the alteration products of uraninite in the Xiazhuang ore-field and the elevated calcium concentration expected in the near-field of nuclear waste repositories due to cement/water reaction, Ca-bearing uranyl silicate (uranophane) and uranyl phosphate (autunite) should be the predominant alteration products almost as soon as the exposure of spent fuel to groundwater in an oxidizing environment.

4.3 Compositional variation of uranyl phases

The major compositions of the uranyl minerals in the Xiazhuang ore field usually deviate considerably from their respective nominal compositions. For example, the Ca : Si : U atomic ratios of uranophane in samples 333-0 and 333-12 are 0.51 : 1.33 : 1 and 0.49 : 1.36 : 1, respectively, with the Si content 30% higher than its stoichiometric value. For the yingjiangite in samples 330-4 and 330-7, the K_2O content is only about 1/3 of that indicated by its structural formula.

On the other hand, XRD patterns indicate that the compositional variation of the uranyl phases does not result in significant structural change. Actually, based on the previously reported composition data, the cation atomic ratios of natural uranyl phases often deviate significantly from their respective stoichiometric values [19, 21, 31, 35, 38]. Moreover, synthesized U^{6+} phases, though confirmed using XRD, often do not have the desired composition [39–41]. These observations demonstrate that significant compositional variation in uranyl minerals is a common phenomenon, although the exact mechanisms causing the observed compositional variation are not well understood. Theoretically, the main mechanisms include structural defect, isomorphous substitution and dehydration. Thus, the structure of U^{6+} minerals would easily be adjusted to accommodate impurity elements.

In uranyl phases, the U^{6+} cation usually occurs as part of an approximately linear $(U^{6+}O_2)^{2+}$ uranyl ion, and the uranyl ion is coordinated by four, five or six anions in an approximately planar arrangement essentially perpendicular to the linear uranyl ion, giving square ($Ur\phi_4$), pentagonal ($Ur\phi_5$) and hexagonal bipyramids ($Ur\phi_6$), respectively [42]. The uranyl-ion oxygens (O_{Ur}) located at two apices of the

bipyramids obtain bond-valences of about 1.79 valence units (vu) from $U^{6+}-O_{Ur}$ bond [43], thus the bonding requirements of the O_{Ur} anions are largely satisfied by the $U^{6+}-O_{Ur}$ bond. However, the equatorial anions receive only ~ 0.5, ~ 0.4 and 0.33 vu from the U^{6+} cation at the center of $Ur\phi_4$, $Ur\phi_5$ and $Ur\phi_6$ polyhedra, respectively. As such, the equatorial anions are often bonded to other cations (U^{6+}, Si^{4+}, or P^{5+}) of high bond-valences, resulting in the polymerization of high bond-valence polyhedra dominantly in two dimensions [42, 43]. As a consequence, all the uranyl minerals found in Xiazhuang ore-field contain sheets that are formed by the polymerization of high bond-valence polyhedra, and the sheets are connected by interlayer low-valence cations and/or hydrogen bonds. Thus, substitution and vacancies may occur at the interstitial sites [44], which may account for the variation of interstitial cations in the structures of the U^{6+} minerals.

Burns *et al.* (1996) [42] have proposed a structural hierarchy for U^{6+} minerals and inorganic phases and, based on 106 phases with sheet structures, grouped the sheets according to the topological arrangement of anions in the sheet. Based on this research, sheets that are compositionally quite different may have similar connectivity. For example, the anion topology of the sheets in schoepite and fourmarierite is the same and resembles that of α-U_3O_8 based on which the sheets of becquerelite and protasite forms; moreover, sixteen structures including uranyl silicates, phosphates, arsenates *etc.*, contain sheets that are based on uranophane anion-topology, and the connectivity of the sheets in uranophane and ulrichite, $Cu[Ca(UO_2)(PO_4)_2](H_2O)_4$, are strikingly similar. The similarity in the connectivity of sheets with quite different compositions could facilitate the compositional variation of uranyl phases while maintaining their respective structure types.

4.4 Trace element behavior during the alteration of uraninite

In addition to the oxidation of U^{4+} to U^{6+}, which takes more oxygen into the structure, a significant amount of H_2O is added to the uranyl phases formed during the oxidative alteration of uraninite. Moreover, as the prevailing secondary phases change from uranyl oxide hydrate to uranyl silicates or phosphates, more and more cation oxides (CaO, SiO_4 or P_2O_5) other than UO_3 will be added into the structure. As a result, the alteration process has a dilution effect on the concentration of both uranium and trace elements, *i.e.*, even if the total amount of uranium and trace elements from the uraninites are transferred into uranyl phases, they will still have a lower content after alteration. Consequently, it is inadequate to determine the mobility of trace elements by directly comparing their contents in uraninite and in the alteration products. Thus, the trace element content in uranyl minerals was normalized using uranium content in this study to reveal their mobility relative to uranium. The uranium-normalized content of a metal (Me) is calculated using the following formula:

$$\mathrm{Me-N} = \frac{\mathrm{Me}}{\mathrm{U_S}} \times \mathrm{U_P}$$

where Me – N is the uranium-normalized content of Me; Me is the EMPA content of Me; U_P is the average EMPA content of uranium in the primary uraninites and U_S is the EMPA content of uranium in secondary minerals.

Lead in uraninite is mainly produced by the radioactive decay of uranium and is incompatible in the structure [29]. Because the oxidative alteration took place most recently when the ore bodies became shallowly buried, and the half-life for the nuclides of uranium is very long (7.0366×10^8 years for ^{235}U and 4.4673×10^9 years for ^{238}U), little radiogenic lead is produced in the uranyl phases, which accounts for the much lower content of lead in most secondary phases except for a few structures (fourmarierite, calciouranoite) which essentially contain significant amounts of lead.

Th, Zr and rare earth elements (REE) are chemical analogues widely used in studying the geochemical behavior of actinides present in high level nuclear waste [45–47], *i.e.*, Th^{4+}, Zr^{4+} and Ce^{4+} are analogues of An^{4+} (An: actinides) and the trivalent REEs are analogues of An^{3+}. In general, the content of Zr and Th is close to or below the EMPA detection limit in the uranium minerals from the Xiazhuang ore field, while that of Y and LREE is higher (Table 2). Yttrium content in uraninite is relatively high with an average of 0.35 wt. % and decreases significantly in the alteration products (0.18% in uranyl oxide hydrate, 0.03% in uranyl silicate and phosphate). However, the contents of Sm^{3+}, Nd^{3+}, Eu^{3+} and Gd^{3+} have a large variation, with the highest contents in the uranyl minerals considerably higher than their respective highest contents in the uraninites, and the uranium-normalized $\sum$LREE in the secondary uranyl phases is slightly higher than that in uraninite. Zirconium is usually below the EMPA detection limit in the uraninite, but is detectable in some uranyl phases with the highest content in yingjiangite up to 0.05 wt. %. Thorium is usually below detection limits in both uraninite and its alteration products. According to the variation of uranium normalized contents of these trace elements in the uranium-minerals from the Xiazhuang ore deposit (Table 2), it could be concluded that Y^{3+} is progressively depleted, and Zr^{4+} and LREEs are enriched as the alteration proceeds from uraninite sequentially to uranyl oxyhydroxide and uranyl silicate or phosphate. The geochemical behavior of these cations can be explained based mainly on their crystallo-chemistry in uranyl phases.

Based on crystal-chemical considerations, Burns *et al.* [12] suggested that An^{5+} and An^{4+} might be incorporated into U^{6+} phases as impurities by substituting for U^{6+}, while An^{3+} might substitute for the large cations at interstial sites. Thus, Zr^{4+} and Ce^{4+} most probably substitute for U^{6+}, and Y^{3+} and trivalent REE would occupy the interlayer sites in the structure of the sheet uranyl minerals. The coupled substitutions $Zr^{4+}(Ce^{4+}) \leftarrow\rightarrow U^{6+}$ and $REE^{3+} \leftarrow\rightarrow Ca^{2+}$ are proposed to be the major mechanism to maintain the charge balance in the structure. The compatibility of a specific cation in the U^{6+} mineral structure would depend on its ionic radius which is provided by Shannon [48].

The interlayer cation of the U^{6+} minerals in the Xiazhuang ore field is dominated by Ca^{2+}. The ion radius of Ce^{3+}, Pr^{3+} and Nd^{3+} in the trivalent REE cations are closest to that of Ca^{2+}, suggesting that the incorporation of these cations into the uranyl minerals might occur easily. On this account, the much smaller ionic radius of Y^{3+} should be responsible for the progressive depletion of yttrium during the

alteration processes. The geochemical behavior of REE^{3+} depends largely on ionic radius which decreases as atomic number increases due to the lanthanide contraction. Yttrium is grouped with the REE due to its close similarity to lanthanides in geochemistry and can be placed between Dy and Er according to its ionic radius in depicting REE distribution patterns. The depletion of yttrium in U^{6+} phases may imply that incorporation of heavy REE into the uranyl phases is not favored in the structures. Therefore, U^{6+} phases are most probably characterized by selective enrichment of LREE.

Natural zircon usually contains significant amount of U^{4+}, suggesting the similarity of Zr^{4+} and U^{4+} in crystallochemistry of zircon. The radius of Zr^{4+}, however, is significantly different from that of U^{4+} and is similar to that of U^{6+}, resulting in a higher Zr^{4+} content in U^{6+} phases than in uraninite.

In addition to the general similarity in the geochemistry of An^{3+} and REE^{3+}, the ionic radii of Am^{3+}, Cm^{3+} and Pu^{3+} are very close to those of trivalent LREE and Ca^{2+}, suggesting that these actinide ions would easily be incorporated into calcium uranyl oxide hydrates, uranophane and autunite which are expected to dominate the alteration products of spent UO_2 fuel by replacing the Ca^{2+} at interlayer sites. On the other hand, the $U^{6+}-O_{Ur}$ bond length is less than 1.90 Å [43], while the ionic distance obtained by summing the crystal radius of U^{6+} and O^{2-} is in the range of 2.17 Å and 2.22 Å. Therefore, U^{6+} can hardly be substituted by larger ions. The ionic radius of An^{4+} is significantly larger than that of U^{6+}, thus the substitution $An^{4+} \leftrightarrow U^{6+}$ requires both an adequate charge-balance mechanism and a significant distortion of the coordination polyhedra. Consequently, this kind of substitution is not expected to occur in any significant amount.

5. Conclusion

1. Abundant uranyl mineral phases occur as alteration products of uraninite in the Xiazhuang uranium ore deposit, China. The alteration products are predominated by the most stable minerals (uranophane for silicate series, autunite and yingjiangite for phosphate series) with minor metastable uranyl oxide hydrates being occasionally found.
2. In granite-hosted nuclear waste repositories where enhanced calcium concentration is expected due to cement/water reactions, uranophane and autunite should be the predominant alteration products of spent UO_2 fuel under oxidizing conditions.
3. The compositions of uranyl phases usually deviate considerably from their respective nominal formulae, suggesting that the structure of uranyl phases, especially those with uranophane anion-topology, might easily be adjusted to accommodate crystallographically compatible elements as impurities.
4. Compared with the primary uraninites, the secondary uranyl minerals would accommodate a little bit more LREE, but significantly less Y^{3+} probably due to its cation-radius mismatch with interlayer Ca^{2+}. Because the ionic radius of Am^{3+}, Cm^{3+} and Pu^{3+} is close to that of trivalent LREE and Ca^{2+}, these actinide ions would substitute for the Ca^{2+} at interlayer sites. However, an adequate charge balance mechanism and significant distortion of the coordination polyhedra are required for the substitution $An^{4+} \leftrightarrow U^{6+}$, so that this type of substitution may not be common.
5. During the oxidative alteration of spent UO_2 fuel, the release rate of An^{3+} is expected to be similar to or slightly lower than that of uranium, while An^{4+} would release at a higher rate than uranium.

Acknowledgment. This work was supported by the Natural Science Foundation of China (grant 40 072 095), and Natural Science Foundation of Guangdong province, China (grant 000 898). EMPA and BSEI were performed in the Electron Microbeam Analysis Facility of State Key Laboratory for Mineral Deposits Research, Nanjing University, and XRD analyses were completed in Department of Earth Sciences, Nanjing University.

References

1. Barner, J. O.: Characterization of LWR spent fuel MCC-approved testing material-ATM-101. Richard, WA PNL-5109: Rev. 1 UC-70. Richard, WA: Pacific Northwest Laboratory (1985).
2. Oversby, V. M.: Nuclear waste materials. In: *Nuclear Materials*. Vol. 10b (Frost, B. R. T., ed.) Material Science and Technology, a comprehensive treatment. VCH, Weinheim, Germany (1994).
3. Frondel, C.: Systematic mineralogy of uranium and thorium. U.S. Geol. Survey Bull. 1064 (1958).
4. Finch, R. J., Ewing, R. C.: J. Nucl. Mater. **190**, 133 (1992).
5. Shoesmith, D. W., Sunder, S.: J. Nucl. Mater. **190**, 20 (1992).
6. Sunder, S., Shoesmith, D. W., Kolar, M., Leneveu, D. M.: From laboratory exoeriments to geological vault: calculation of used nuclear fuel dissolution rates. In: Scientific Basis for nuclear waste management XXI. Mater. Res. Soc. Proc. **506**, 273 (1998).
7. Bruno, J., Cera, E., Duro, L., Ericksen, T. E., Werme, L. O.: J. Nucl. Mater. **238**, 110 (1996).
8. Finn, P. A., Hoh, J. C., Wolf, S. F., Eleckis, E., Tani, B. S.: Radiochim. Acta **74**, 65 (1996).
9. Wronkiewicz, D. Z., Bates, J. K., Wolf, S. F., Buck, E. C.: J. Nucl. Mater. **238**, 78 (1996).
10. Hedin, A.: Nucl. Technol. **138**, 179 (2002).
11. Chen, Y. T.: Comput. Geosci. **29**, 385 (2003).
12. Burns, P. C., Ewing R. C., Miller, M. L.: J. Nucl. Mater. **245**, 1 (1997).
13. Chen, F. R., Burns, P. C., Ewing, R. C.: J. Nucl. Mater. **275**, 81 (1999).
14. Douglas, M., Clark, S. B., Friese, J. I., Arey, B. W., Buck, E. C., Hanson, B. D.: Env. Sci. Technol. **39**, 4117 (2005).
15. Smellie, J. A. T., Karlson, F.: Engin. Geol. **52**, 193 (1999).
16. Petit, J. C.: Radiochim. Acta **52**/**53**, 337 (1991).
17. Janeczek, J., Ewing, R. C., Oversby V. M., Werme L. O.: J. Nucl. Mater. **238**, 121 (1996).
18. Finch, R. J., Ewing, R. C.: Radiochim. Acta **52**/**53**, 395 (1991).
19. Isobe, H., Murakami, T., Ewing, R. C.: J. Nucl. Mater. **190**, 174 (1992).
20. Pearcy, E. C., Prikryl, J. D., Murphy, W. M., Leslie, B. W.: Appl. Geochem. **9**, 713 (1994).
21. Zhao, D. G., Ewing, R. D.: Radiochim. Acta **88**, 739 (2000).
22. Jensen, K. A., Palenik, C. S., Ewing, R. C.: Radiochim. Acta **90**, 761 (2002).
23. Bros, R., Hidaka, H., Kamei, G., Ohnuki, T.: Appl. Geochem. **18**, 1807 (2003).
24. Xu, D. Zh., Xue, Zh. H.: Uranium Geol. **10**(3), 150 (1994) (in chinese with english abstract).
25. Liu, J. H., Li, X. L.: J. East China Geol. Inst. **21**(4), 330 (1998) (in chinese with english abstract).
26. Yang, Y. X., Liu, Q. C., Long, Q. H., Deng, J. Zh., Wu, L. Q., Yin, Zh. P.: Geophys. Geochem. Explor. **27**(3), 184 (2003) (in chinese with english abstract).

27. Wu, L. Q., Tan, Zh. Zh., Liu, R. Zh., Huang, G. L.: Uranium Geol. **19**(1), 28 (2003) (in chinese with english abstract).
28. Xu, D. Zh., Liu, L. Q., Hu, B. Q.: Uranium Geol. **15**(5), 266 (1999) (in chinese with english abstract).
29. Janeczek, J., Ewing, R. C.: Geochim. Cosmochim. Acta **59**, 1917 (1995).
30. Janeczek, J., Ewing, R. C.: J. Nucl. Mater. **190**, 128 (1992).
31. Fayek, M., Kyser, T. K.: Can. Mineral. **35**, 627 (1997).
32. Smith, D. K., Scheetz, B. E., Anderson, C. A. F., Smith, K. A.: Uranium **1**, 79 (1982).
33. Langmuir, D.: Geochim. Cosmochim. Acta **42**, 547 (1978).
34. Cheng, Zh. R., Huang, Y. Zh., Gu, X. F.: Acta Minral. Sinica **10**(2), 102 (1990) (in chinese with english abstract).
35. Zhang, J. Y., Wan, A. W., Gong, W. Sh.: Acta Petrol. Mineral. **11**(2), 178 (1992) (in chinese with english abstract).
36. Chen, F. R., Ewing, R. C., Clark, S. B.: Am. Mineral. **84**, 650 (1999).
37. Wronkiewicz, D. Z., Bates, J. K., Gerding, T. J., Eleckis, E., Tani, B. S.: J. Nucl. Mater. **190**, 107 (1992).
38. Casas, I., Bruno, J., Cera, E., Finch, R. J., Ewing, R. C.: Geochim. Cosmochim. Acta **61**, 3879 (1997).
39. Haverbeke, L. V., Vochten, R., Springel, K. V.: Mineral. Magazine **60**, 759 (1996).
40. Nguyen, S. N., Silva, R. J., Weed, H. C.: J. Chem. Thermodyn. **24**, 359 (1992).
41. Perez, I., Casas, I., Martin, M.: Cosmochim. Acta **64**, 603 (2000).
42. Burns, P. C., Miller, M. L., Ewing, R. C.: Can. Mineral. **34**, 845 (1996).
43. Burns, P. C., Ewing, R. C., Hawthorne, F. C.: Can. Mineral. **35**, 1551 (1997).
44. Chen, F. R., Ewing, R. C.: Sci. China **46**, 39 (2003).
45. Krauskopf, K. B.: Chem. Geol. **55**, 323 (1986).
46. Iida, Y., Ohnuki, T., Isobe, H.: J. Contamin. Hydrol. **35**, 191 (1998).
47. Hidaka, H., Gauthier-Lafaye, F.: Geochim. Cosmochim. Acta **64**, 1093 (2000).
48. Shannon, R. D.: Acta Cryst. A **32**, 751 (1976).